International Journal of Nanomedicine

Dovepress
open access to scientific and medical research

Open Access Full Text Article

ORIGINAL RESEARCH

# Three-photon imaging using defect-induced photoluminescence in biocompatible ZnO nanoparticles



Achyut J Raghavendra[1]
Wren E Gregory[1]
Tyler J Slonecki[2]
Yongchang Dong[1]
Indushekhar Persaud[3]
Jared M Brown[3]
Terri F Bruce[2]
Ramakrishna Podila[1,4]

[1]Laboratory of Nano-Biophysics, Department of Physics and Astronomy, Clemson Nanomaterials Institute, Clemson University, Clemson, SC, USA; [2]Clemson Light Imaging Facility, Clemson University, Clemson, SC, USA; [3]Department of Pharmaceutical Sciences, Skaggs School of Pharmacy and Pharmaceutical Sciences, University of Colorado-Anschutz Medical Campus, Aurora, CO, USA; [4]Clemson University School of Health Research and COMSET, Clemson University, Clemson, SC, USA



**Background:** Although optical spectroscopy promises improved lateral resolution for cancer imaging, its clinical use is seriously impeded by background fluorescence and photon attenuation even in the so-called two-photon absorption (2PA) imaging modality. An efficient strategy to meet the clinical cancer imaging needs, beyond what two-photon absorption (2PA) offers, is to use longer excitation wavelengths through three-photon absorption (3PA). A variety of fluorescent dyes and nanoparticles (NPs) have been used in 3PA imaging. However, their nonlinear 3PA coefficient is often low necessitating high excitation powers, which cause overheating, photodamage, and photo-induced toxicity. Doped wide band gap semiconductors such as Mn:ZnS NPs have previously been used for 3PA but suffer from poor 3PA coefficients.

**Methods:** Here, we prepared ZnO NPs with intrinsic defects with high 3PA coefficients using a polyol method. We functionalized them with peptides for selective uptake by glioblastoma U87MG cells and used breast cancer MCF-7 cells as control for 3PA studies. Uptake was measured using inductively coupled plasma-mass spectrometry. Biocompatibility studies were performed using reactive oxygen species and cell viability assays.

**Results:** We demonstrate that ZnO NPs, which have a band gap of 3.37 eV with an order of magnitude higher 3PA coefficients, can facilitate the use of longer excitation wavelengths 950–1,100 nm for bioimaging. We used the presence intrinsic defects (such as O interstitials and Zn vacancies) in ZnO NPs to induce electronic states within the band gap that can support strong visible luminescence 550–620 nm without the need for extrinsic doping. The peptide functionalization of ZnO NPs showed selective uptake by U87MG cells unlike MCF-7 cells without the integrin receptors. Furthermore, all ZnO NPs were found to be biocompatible for 3PA imaging.

**Conclusion:** We show that defect-induced luminescence 550–620 nm in ZnO NPs (20 nm) due to 3PA at longer excitation (975 nm) can be used for 3PA imaging of U87MG glioblastoma cells with lower background noise.

**Keywords:** three-photon imaging, ZnO nanoparticles, defects, photoluminescence

## Introduction

High-resolution imaging techniques that delineate tumors and calcifications from normal tissue play an important role in cancer diagnosis and treatment.[1–3] While many imaging techniques, such as computed tomography (CT), single-photon emission computed tomography (SPECT), positron emission tomography (PET), intraoperative/functional magnetic resonance imaging (MRI) and ultrasound, have been widely used in clinical and preclinical trials, no single technique is suited for addressing all clinical needs in terms of imaging depth and lateral resolution.[1,4] For example, ultrasound, CT, MRI, PET and SPECT can probe deep into the tissue but suffer from poor spatial resolution (>1 mm). In contrast, multi-photon fluorescence imaging, which uses either intrinsic fluorescence

Correspondence: Ramakrishna Podila
Laboratory of Nano-Biophysics, Department of Physics and Astronomy, Clemson Nanomaterials Institute, Clemson University, 81 Technology Drive, Suite 200, Anderson, SC 29625, USA
Tel +1 864 656 4447
Fax +1 864 656 3416
Email rpodila@g.clemson.edu

submit your manuscript | www.dovepress.com
Dovepress
http://dx.doi.org/10.2147/IJN.S165201

of biomolecules or fluorescent contrast agents to identify diseased structures, has a great potential for detecting small size tumors that could be otherwise missed using traditional techniques such as MRI.[5,6] Multi-photon imaging uses near-infrared (NIR) excitation wavelengths in the so-called optical transparency window (700–1,100 nm) of biological tissues to mitigate light scattering and auto-fluorescence effects for deeper penetration. In particular, it has long been known that three-photon absorption (3PA) imaging with NIR excitation can penetrate through several millimeters of tissue and provide at least an order of magnitude higher resolution relative to one- and two-photon imaging.[7] The disadvantage with this modality, however, is that the 3PA process is a highly non-linear optical phenomenon, and usually requires very high powers at which photobleaching and phototoxicity from conventional dyes (eg, methylene blue) with low 3PA coefficients become significant concerns.[8,9] In order to accurately identify tumors and resection margins without photobleaching and background noise via 3PA imaging, it is imperative to achieve 3PA probes with three characteristics: 1) a high 3PA coefficient at low laser powers comparable to one- and two-photon imaging (1–10 mW); 2) a strong luminescence emission in the visible/NIR region with little or no photobleaching; and 3) a low immune/allergic response and no toxicity.

In the past decade, many nanomaterials (NMs; eg, Au/Ag nanorods and semiconductor quantum dots [QDs] such as CdSe and CdS) have been developed for in vitro and in vivo 3PA imaging.[10,11] However, the use of NMs has been impeded by their inability to simultaneously satisfy the characteristics listed above. For instance, CdSe and CdS exhibit strong optical absorption but the presence of Cd results in undesired toxicity.[12,13] Similarly, Au/Ag nanostructures scatter light strongly and could lead to phototoxicity from plasmon-induced heat generation. Furthermore, the intrinsic 3PA coefficients of many existing NMs decrease rapidly at higher excitation wavelengths, making it challenging to achieve deeper penetration for imaging.

Wide bandgap semiconductors such as ZnO and ZnS, exhibit excellent biocompatibility with strong 3PA coefficients in the NIR region and could be ideally suited for 3PA imaging if strong visible/NIR photoluminescence is induced. Recently, Yu et al overcame this challenge by doping ZnS nanocrystals with Mn to elicit visible photoluminescence for 3PA imaging.[8] In their studies, a simultaneous absorption of three photons at 920 nm was used to excite Mn-doped ZnS nanocrystals, resulting in a photoluminescence peak, ~580 nm. They conjugated luminescent ZnS:Mn nanocrystals with arginine–glycine–aspartic acid (RGD) for targeted uptake to image melanoma and breast cancer.[8] While ZnS:Mn nanocrystals show promising properties for 3PA imaging, ZnS exhibits a large band gap, ~3.7 eV (maximum excitation wavelengths: ~920–950 nm), and cannot utilize longer wavelengths (950–1,040 nm) in the traditional Ti:Sapphire laser spectrum. Furthermore, the 3PA coefficients of ZnS are low (~$20 \times 10^{-4}$ $cm^3/GW^2$ for 780–860 nm range) due to its relatively larger band gap.[14,15] Given that the 3PA coefficients decrease with increasing wavelength (see Figure S1), the use of ZnS nanocrystals is disadvantageous at longer wavelengths (>900 nm) for meeting the first need, because higher laser powers (≥10 mW) become essential to compensate for their low 3PA coefficient.[8]

Here, we demonstrate that ZnO nanoparticles (NPs) can simultaneously meet the three needs for 3PA imaging. ZnO NPs exhibit a lower band gap, ~3.37 eV, compared to ZnS and thereby facilitate the use of longer excitation wavelengths, ~950–1,100 nm. Unlike other wide band gap materials such as $TiO_2$ with an indirect gap, the presence of intrinsic defects (such as O interstitials and Zn vacancies) in ZnO NPs induces electronic states within the band gap that can support strong visible luminescence without the need for extrinsic doping. More importantly, the 3PA coefficients of ZnO NPs are at least 8–10 times larger than ZnS (used previously[8]) in the near-infrared region (Figure S1), which allows imaging at significantly lower powers (~5 mW) that are comparable to traditional two-photon imaging (1–10 mW). In this article, we show that pristine and RGD-functionalized ZnO NPs (~20 nm) synthesized using a polyol method display strong visible luminescence, ~550–620 nm, with high 3PA coefficients. The RGD peptides functionalization was used to selectively target $\alpha_v\beta_3$ integrin receptors in U87MG glioblastoma. While integrin-negative MCF-7 breast cancer cells did not show any selective uptake, U87MG glioblastoma cells exhibited increased uptake of RGD-functionalized ZnO NPs. As a proof-of-concept, a three-photon excitation, ~975 nm, was successfully used to image U87MG glioblastoma in vitro through the defect-induced visible luminescence, ~550–620 nm, from ZnO NPs. Lastly, no significant changes were found in in vitro cell viability confirming the biocompatibility of ZnO NPs.

## Material and methods

All the chemicals used were purchased from Sigma-Aldrich Co. (St Louis, MO, USA) unless mentioned otherwise. ZnO NPs were synthesized by slowly heating zinc acetate dehydrate and polyvinylpyrrolidone (PVP, 10,000 g/mol) dissolved in diethyleneglycol (DEG) to 180°C.[16] De-ionized water was injected drop-wise into hot zinc acetate-dissolved DEG solution using a syringe pump at a constant rate of 1 mL/s to induce nucleation of ZnO NPs indicated by the

formation of a white precipitate. The reaction was stopped after 30 mins. NPs were separated from the liquid by centrifugation (15,000 rpm) and then washed repeatedly with methanol to remove PVP and DEG. Subsequent centrifugation was used to remove methanol and the ZnO NPs were resuspended in DI water. The obtained ZnO NPs were characterized using transmission electron microscopy (TEM; Hitachi-7600, Hitachi Ltd, Tokyo, Japan), as shown in Figure 1A. The mean diameter was found to be ~22±5 nm. ZnO NPs were functionalized using tumor-targeting c(RGDyK) peptides through a traditional thiol-maleimide reaction.[17] To this end, ZnO NPs (2.5 mg/mL) were bath sonicated with 3-mercaptopropionic acid (1.5 mg/mL) in dichloromethane (DCM) to introduce thiol groups onto the surface. For adding maleimide (a thiol-reactive group) onto c(RGDyK) peptides (for selective binding of $\alpha_v\beta_3$ integrin on U87MG cells), maleimide poly(ethylene glycol) succinimidyl carboxy methyl ester (Mal-PEG-SCM; 5 mg/mL; purchased from Creative PEGWorks, Durham, NC, USA) was reacted with the c(RGDyK) peptide (0.75 mg/mL), in phosphate buffer saline for 4 h at room temperature. Subsequently, thiolated ZnO NPs (0.2 mg/mL) were added to the Mal-PEG-SEM and c(RGDyK) mixture and stirred for 1 hr in the presence of tris(2-carboxyethyl)phosphine hydrochloride (TCEP; 0.5 mg/mL). TCEP significantly increases the acidity of the solution and 3 M NaOH solution was added to neutralize the solution to pH ~7.2. Functionalized ZnO NPs were confirmed by FTIR spectrum as shown in Figure S3.

Single-photon photoluminescence (PL) studies were performed using Horiba-Jobin Yvon Nanolog (excitation: 325 nm). X-ray photoemission spectroscopy (XPS) measurements were performed using a Kratos Axis Ultra DLD instrument calibrated through C 1 s peak at 284.6 eV. Linearly polarized 7 ns optical pulses from a Q-switched

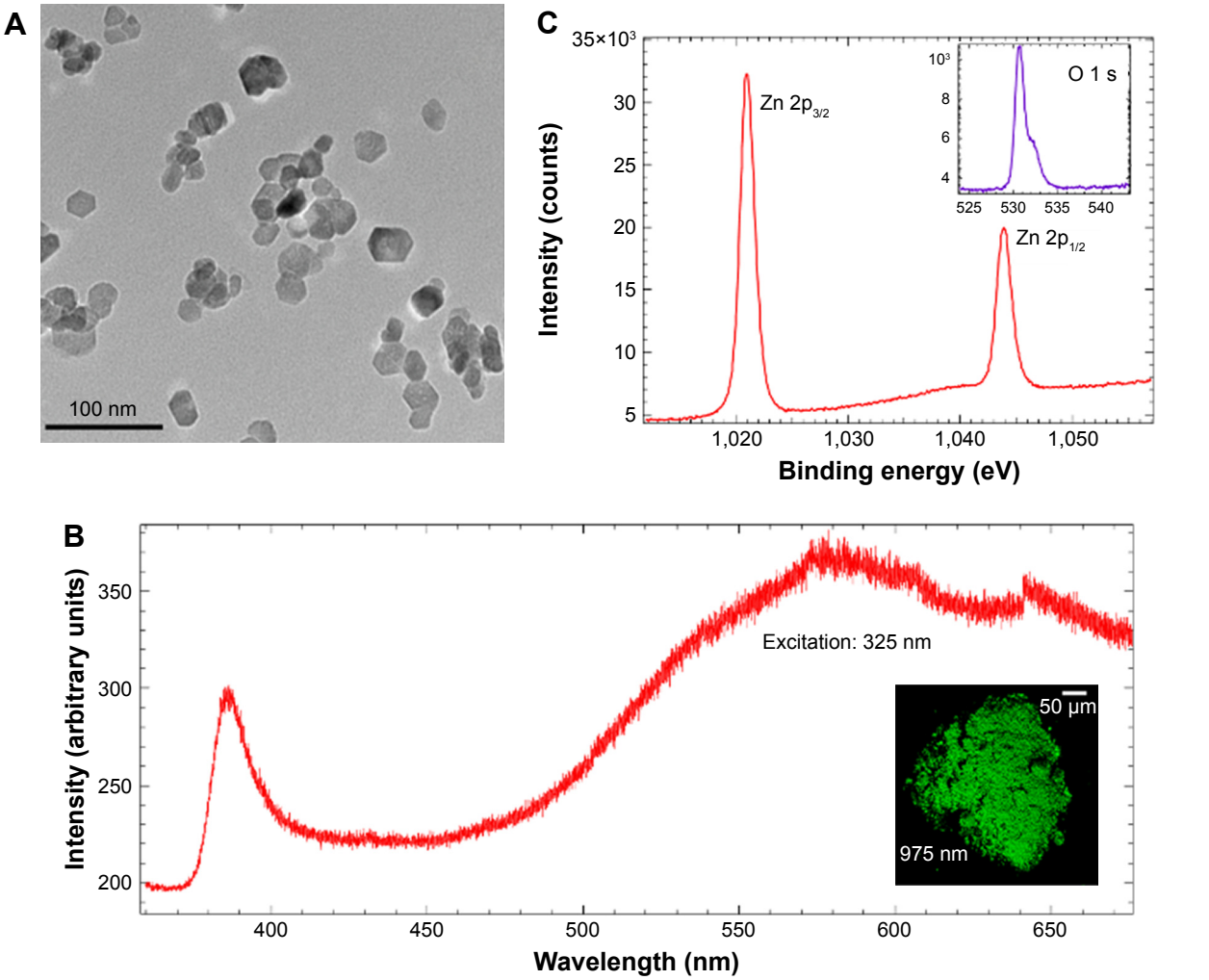


**Figure 1** (**A**) A representative transmission electron micrograph for ZnO NPs prepared using the polyol method. (**B**) Single-photon excitation ~325 nm (resonant with ZnO band gap) photoluminescence from ZnO NPs shows ultra-violet (UV) emission arising from the band-edge along with more intense broad visible emission from intrinsic defects between 500 and 650 nm. The inset shows a multiphoton microscope image of Zn NPs visible luminescence excited with ~975 nm three-photon equivalent of ZnO band gap. (**C**) X-ray photoelectron spectra of Zn and O (shown in the inset) showed that the as-prepared ZnO NPs are non-stoichiometric with Zn vacancies.

frequency-doubled Nd:YAG laser (Surelite, Coherent Lasers, Santa Clara, CA, USA) at 1,064 nm were used for obtaining 3PA coefficients. The position dependent transmittance was measured using two calibrated photodetectors (Rjp-225; Laser Probe, Inc, Utica, NY, USA): one for incident and another for transmitted light. The value of the 3PA coefficient was obtained by numerically fitting the Z-scan curve to the 3PA propagation equation, given by $dI/dz' = -\alpha I - \gamma I^3$, where $I$ is the intensity, $\alpha$ and $\gamma$ are 1PA and 3PA coefficients, and $z'$ is the propagation distance within the sample.

Three-photon imaging experiments were performed using a Leica TCS SP8X multiphoton microscope coupled with a Coherent Chameleon Vision S Ti:Sapphire laser (excitation wavelength: 975 nm, average power at the sample ~5.2 mW). Pristine and functionalized ZnO NPs (10 µg/mL) were incubated with U87MG and MCF-7 (integrin-negative) cells for different times and washed thrice to remove unadsorbed NPs, fixed in 4% paraformaldehyde, and covered with PBS:glycerol (50/50, v/v). Images were acquired at 0, 10, 15, 30, and 60 min incubation times. Nikon NIS-Elements image analysis program was used to obtain intensities from at least five different regions of interest for each cell type and averaged to find the mean intensity.

To test the in vitro biocompatibility, RAW 264.7 mouse macrophage cells (American Type Culture Collection, Manassas, VA, USA) were seeded in 96-well plates (20,000 cells per well) and grown to 80% confluency before exposure to ZnO NPs (3.125, 6.25, 12.5, 25, 50 µg/mL). After 24 hrs of exposure to ZnO, cells were washed with phosphate-buffered saline and phenol-free media was added to each well. Reagent from CellTiter 96® Aqueous One Solution Cell Proliferation Assay was added to each well and the plate was incubated for 45 min before absorption was measured on a Biotek plate reader. Viability was compared to the control group. For evaluation of reactive oxygen species (ROS) generation, RAW cells were exposed to ZnO NPs (3.125, 6.25, 12.5, 25, 50 µg/mL) for 45 min in 24-well plates. Cells were trypsinized, pelleted, and washed with PBS three times. DCF reagent was purchased from Molecular Probes, Eugene, OR, USA (CM-H2DCFDA: Cat#C6827) and added to the RAW cells in PBS. Cells were incubated at 37°C for 30 min before measuring the mean fluorescence using flow cytometry (Accuri C6).

## Results and discussion

The mean diameter of ZnO NPs was found to be 22±5 nm using TEM (see Figure 1A). While as prepared ZnO NPs had a low zeta potential, ~−11 mV, peptide functionalized ZnO NPs (pep-ZnO NPs) showed better stability, ~−22 mV, in deionized water. Single-photon PL studies showed a prominent band-edge emission at 380 nm with 325 nm excitation (~3.3 eV) in addition to a broad visible emission between 500 and 650 nm due to the presence of defects (Figure 1B). The Zn 2p core-level in the XPS of ZnO NPs (Figure 1C) displayed two peaks located at ~1,021 and 1,044 eV, which may be attributed to Zn $2p_{3/2}$ and Zn $2p_{1/2}$, respectively. On the other hand, O 1 s displayed two peaks located at 530.5 and 532 eV, which belong to the Zn–O bonding in ZnO and C=O peak arising from the surface adsorbed acetate from the decomposition of zinc acetate during the synthesis. The results showed that the ratio of O/Zn is slightly higher than unity ~1.06, suggesting the presence of Zn vacancies ($V_{Zn}$), O interstitials ($O_i$), and anti-sites ($O_{Zn}$). It is worth noting that Zn vacancies and O anti-sites are expected to be more predominant, as only a few O interstitials could be present due to the large size of O atoms. When taken together, PL and XPS results reveal that the Zn vacancies induce mid-gap states within the band gap of ZnO NPs (see Figure S2) and mediate visible photoluminescence.

In wide band gap semiconductors such as ZnO and ZnS, 3PA could occur either through genuine absorption involving simultaneous absorption of three photons with transition from the valence to conduction band via virtual states, or an excited state absorption (ESA) involving sequential absorption of three photons via real defect-induced mid-gap electronic states.[18,19] We previously showed that the presence of mid-gap states, provided by defects such as Zn vacancies, increases the transition probability of photo-excited electrons and thus enhances the 3PA co-efficient in ZnO NPs.[19] As mentioned earlier, higher 3PA coefficients are advantageous, because they allow imaging at lower powers (<10 mW). Detailed Z-scan measurements (Figure 2A) confirmed the high 3PA coefficients in ZnO NPs due to the presence of defect-induced mid-gap states. In the Z-scan measurement, light-induced changes in transmittance ($\Delta T$) of a medium due to optical nonlinearities such as the multi-photon absorption, are measured as a function of the sample position (z) within the focal region of a focused laser beam. A smooth valley shaped curve, symmetric about the focal point (z = 0), was observed in the Z-scan of ZnO NPs (Figure 2A). The input light intensity, or fluence, changes as a function of z when the sample is translated through the focal region, allowing one to plot $\Delta T$ as a function of the input fluence (Figure 2B). The nonlinear absorption coefficients could be derived from this data through numerical analysis, as discussed in the experimental section. As shown in Figure 2A and B, the best fit to the experimental data was obtained for a 3PA process at different energies with 3PA coefficient, ~0.5 $cm^3/GW^2$.

Returning to Figure 1B, ZnO NPs displayed green luminescence (~550 nm) when excited using three-photon

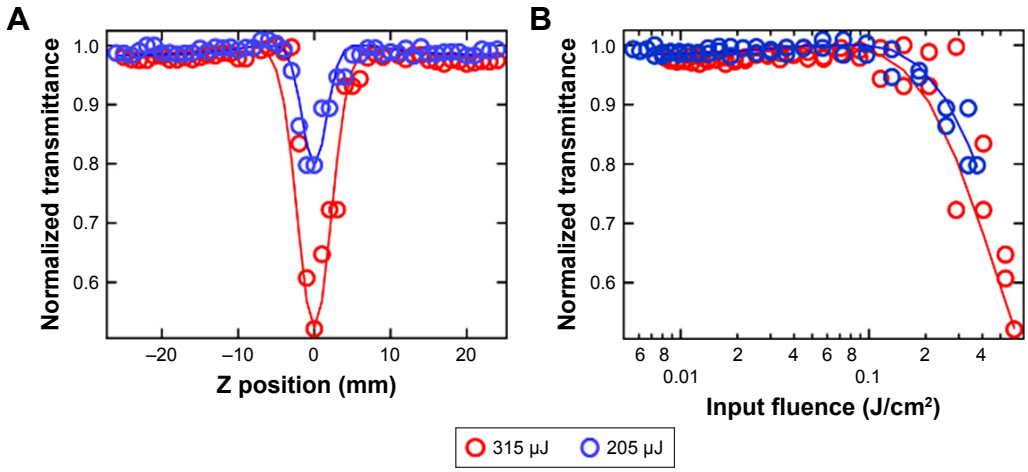


**Figure 2** (**A**) As-obtained Z-scan data for ZnO NPs (shown as open circles) at different incident energies. The solid lines show the fit obtained by numerically solving the three-photon absorption (3PA) equation. (**B**) The Z-scan data for ZnO NPs plotted as a function of input fluence derived from the position dependent data shown in (**A**). The non-linearity in absorption is evident in the rapid decrease in transmission above 0.1 J/cm$^2$.

excitation at 975 nm (~1.25 eV), which is slightly higher than 1/3rd of the band gap energy of ZnO. The green luminescence was previously attributed to the presence of defect-induced surface states within the band gap of ZnO (Figure S2). Many hypotheses, often contradictory, have been proposed to establish relationships between ZnO visible emission and defect-induced states.[20] Based on our results presented in Figure 1, we attribute the visible luminescence of as-prepared ZnO NPs mainly to $V_{Zn}$, $O_{Zn}$, and possibly $O_i$ (Figure S2). Using 3PA imaging, pristine ZnO NPs were observed to physisorb mainly on the surface of MCF-7 and U87MG cells (Figures 3A and B), defining their border with green

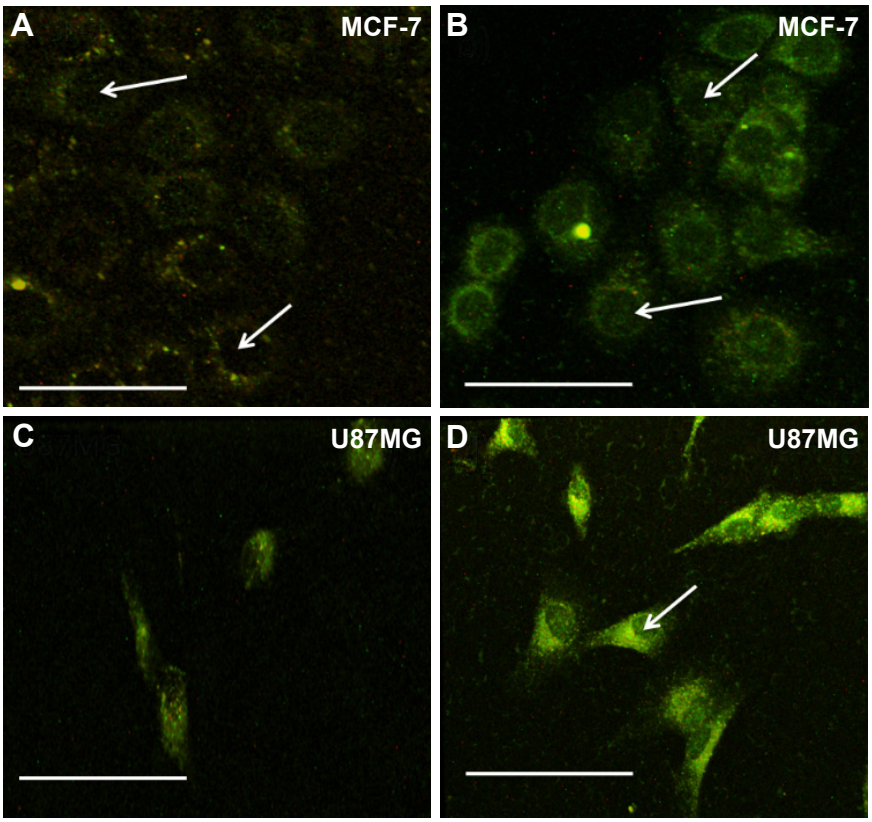


**Figure 3** (**A** and **B**) show three-photon microscopy images for integrin negative MCF-7 cells exposed to pristine and peptide functionalized ZnO NPs respectively. Both as-prepared and pep-ZnO NPs showed exclusive physisorption with little or no cellular uptake as shown by the white arrows. (**C** and **D**) show three-photon microscopy images for integrin positive U87MG cells. Clearly, pep-ZnO NPs exhibited a strong cellular uptake for U87MG cells due to the presence of $\alpha_v\beta_3$-integrin receptors. The scale bars correspond to 50 µm.

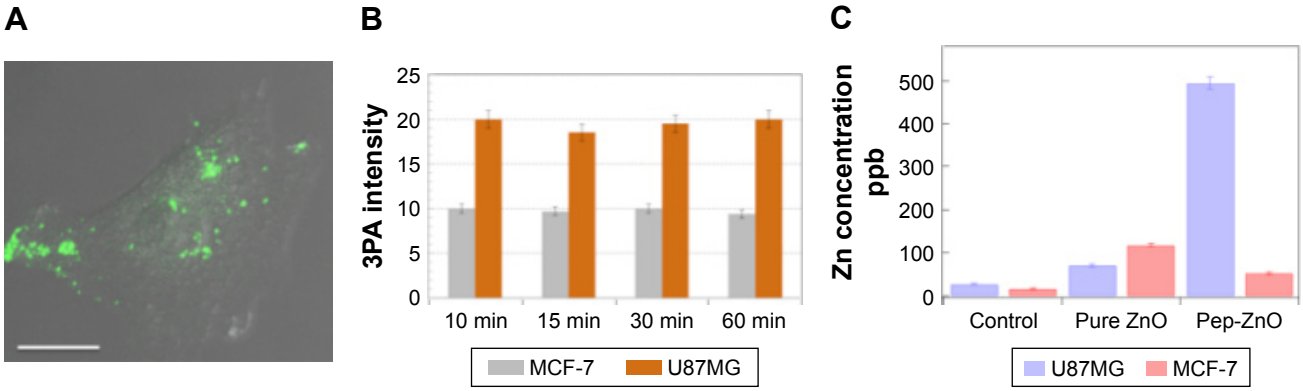


**Figure 4** (**A**) An image showing pep-ZnO NPs endocytosed by U87MG cells through integrin receptors. The background was adjusted to clearly delineate the cell periphery. The scale bar corresponds to 50 µm. (**B**) The mean fluorescence intensity of peptide functionalized ZnO NPs (pep-ZnO) for MCF-7 and U87MG cells at different incubation times. (**C**) ICP-MS measurements for MCF-7 and U87MG cells exposed to pristine and pep-ZnO NPs for 24 hrs confirmed that ZnO NPs uptake was >5 times higher for U87MG exposed to pep-ZnO NPs.

luminescence. This result is expected because bare ZnO NPs lack specific functional groups that can selectively interact with the cell surface receptors to promote their uptake. Upon functionalization with c(RGDyK) peptide (specific for integrin receptors present on the U87MG surface), pep-ZnO NPs were selectively endocytosed by U87MG cells, unlike MCF-7 (Figure 3C and D). While pep-ZnO NPs were found on the surface of MCF-7, no ZnO NPs were seen in the cell cytoplasm as indicated by the arrows in Figure 3C. On the other hand, U87MG cells exhibited excellent uptake due to the selective interaction between c(RGDyK) peptides and $\alpha_v\beta_3$ integrin receptors (Figure 3D and 4A). The differences in the uptake of pep-ZnO NPs were also evident in the average green emission intensity. As expected, we observed a significantly higher average intensity of three-photon luminescence (derived from at least five different spots) for U87MG relative to MCF-7 (Figure 4B) due to specific uptake through $\alpha_v\beta_3$ integrin receptors. To confirm the specific uptake of pep-ZnO NPs by U87MG cells, we performed inductively coupled plasma mass spectrometry (ICP-MS) for determining Zn concentration in U87MG and MCF-7 cells exposed to both pristine and pep-ZnO NPs. As shown in Figure 4C, U87MG clearly showed higher Zn concentrations when exposed to pep-ZnO confirming the selective uptake. Additional 3PA images as a function of incubation time for both MCF-7 and U87MG using bare and pep-ZnO NPs are shown in Figures S4 and S5. The high 3PA coefficients of ZnO NPs enable 3PA imaging at a low power ~5 mW (see Table S1), which is comparable to the power used in traditional two-photon imaging. As mentioned earlier, this is advantageous to avoid photo-induced biological damage and photobleaching effects.

Lastly, the in vitro biocompatibility of ZnO NPs was evaluated using both U87MG and MCF-7 cells. The toxicity of many metal-oxide NPs was previously attributed to the generation of reactive oxygen species (ROS).[21] Accordingly, oxidative stress induced by ZnO NPs (25 µg/mL) was measured in U87MG and MCF-7 cells (see methods for details) with and without laser exposure (at 975 nm excitation used for imaging). No significant changes were observed in the generation of ROS species even at a concentration as high as 25 µg/mL (Figure 5A and B). Also cell viability, which was assessed using MTS assay, showed no significant change in the number of cells viable with functionalized ZnO NPs and bare ZnO NPs (Figure S6).

## Conclusion

In conclusion, ZnO NPs (~22±5 nm) prepared using the polyol method exhibited a high 3PA coefficient, ~0.5 $cm^3/GW^2$, which is 8–10 times larger than other wide band gap imaging agents such as ZnS. In addition to the band edge emission, ~380 nm, intrinsic defects in ZnO NPs (particularly zinc vacancies and O interstitials) resulted in a strong green-orange visible photoluminescence (500–650 nm) for both single- and three-photon excitations without the need for extrinsic dopants. The 3PA images obtained using ZnO NPs, functionalized with peptides, showed selective NP uptake by U87MG glioblastoma through integrin receptors, unlike MCF-7 breast cancer cells. The high 3PA coefficient of ZnO NPs facilitated in vitro 3PA imaging at ~5 mW, one of the lowest powers reported thus far for 3PA imaging modality. ZnO NPs did not exhibit significant toxicity or ROS generation at concentrations used for imaging, confirming that the defect-induced emission in ZnO NPs is ideal for 3PA imaging.

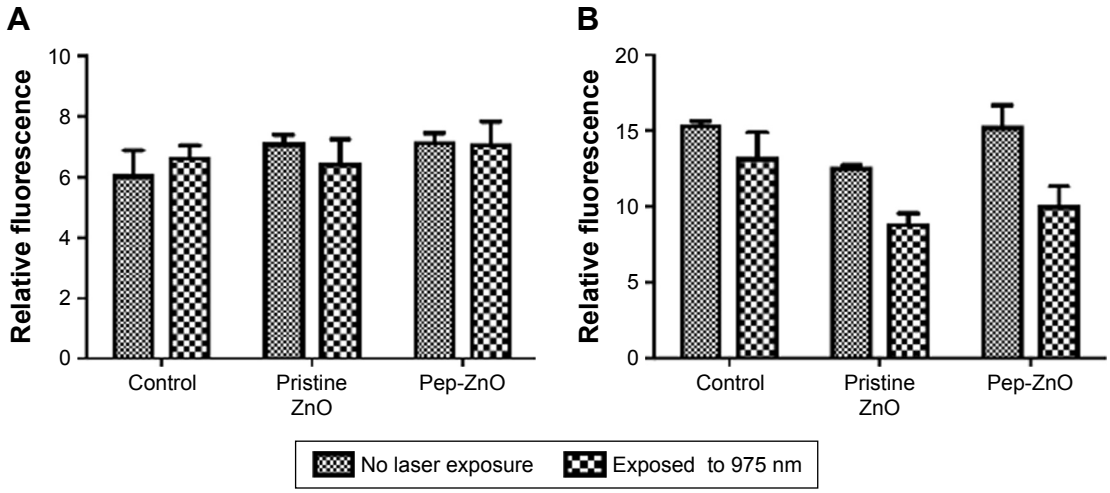


**Figure 5** Changes in reactive oxygen species (ROS) levels in (**A**) MCF-7, and (**B**) U87MG cells following exposure to pristine and peptide-functionalized ZnO NPs at 25 μg/mL for 10 h.

## Acknowledgments

RP and JMB gratefully acknowledge funding support from NIH NIEHS R01-ES019311-07. TFB is thankful to NSF for the MRI award #1126407.

## Author contributions

RP developed the concept. RP, JMB and TFB conceived the experiments. AJR, WEG, TJS, RP and YD prepared samples and carried out experiments. All authors contributed toward data analysis, drafting and revising the paper and agree to be accountable for all aspects of the work. RP supervised the project.

## Disclosure

The authors report no conflicts of interest in this work.

## References

1. Liu JTC, Meza D, Sanai N. Trends in fluorescence image-guided surgery for gliomas. *Neurosurgery*. 2014;75(1):61–71.
2. Gioux S, Choi HS, Frangioni JV. Image-guided surgery using invisible near-infrared light: fundamentals of clinical translation. *Mol Imaging*. 2010;9(5):237–255.
3. Wyckoff J, Gligorijevic B, Entenberg D, Segall J, Condeelis J. High-resolution multiphoton imaging of tumors in vivo. *Cold Spring Harb Protoc*. 2011;2011(10):1167–1184.
4. Yuan B, Rychak J. Tumor functional and molecular imaging utilizing ultrasound and ultrasound-mediated optical techniques. *Am J Pathol*. 2013;182(2):305–311.
5. Kairdolf BA, Bouras A, Kaluzova M, et al. Intraoperative spectroscopy with ultrahigh sensitivity for image-guided surgery of malignant brain tumors. *Anal Chem*. 2016;88(1):858–867.
6. Keating J, Tchou J, Okusanya O, et al. Identification of breast cancer margins using intraoperative near-infrared imaging. *J Surg Oncol*. 2016;113(5):508–514.
7. Xu C, Zipfel W, Shear JB, Williams RM, Webb WW. Multiphoton fluorescence excitation: new spectral windows for biological nonlinear microscopy. *Proc Natl Acad Sci U S A*. 1996;93(20):10763–10768.
8. Yu JH, Kwon S-H, Petrášek Z, et al. High-resolution three-photon biomedical imaging using doped ZnS nanocrystals. *Nat Mater*. 2013;12(4):359–366.
9. Zagorovsky K, Chan WCW. Bioimaging: illuminating the deep. *Nat Mater*. 2013;12(4):285–287.
10. Tong L, Cobley CM, Chen J, Xia Y, Cheng JX. Bright three-photon luminescence from gold/silver alloyed nanostructures for bioimaging with negligible photothermal toxicity. *Angew Chemie Int Ed Engl*. 2010;49(20):3485–3488.
11. Rao J, Dragulescu-Andrasi A, Yao H. Fluorescence imaging in vivo: recent advances. *Curr Opin Biotechnol*. 2007;18(1):17–25.
12. Wang L, Nagesha DK, Selvarasah S, Dokmeci MR, Carrier RL. Toxicity of CdSe nanoparticles in Caco-2 cell cultures. *J Nanobiotechnology*. 2008;6:11.
13. Kauffer FA, Merlin C, Balan L, Schneider R. Incidence of the core composition on the stability, the ROS production and the toxicity of CdSe quantum dots. *J Hazard Mater*. 2014;268:246–255.
14. Gu B, He J, Ji W, Wang HT. Three-photon absorption saturation in ZnO and ZnS crystals. *J Appl Phys*. 2008;103(7):9235–9247.
15. Sreeja R, Sridharan K, Philip R, Jayaraj MK. Impurity mediated large three photon absorption in ZnS:Cu nanophosphors. *Opt Mater*. 2014;36(5):861–866.
16. Lee S, Jeong S, Kim D, Hwang S, Jeon M, Moon J. ZnO nanoparticles with controlled shapes and sizes prepared using a simple polyol synthesis. *Superlattices Microstruct*. 2008;43(4):330–339.
17. Hong H, Shi J, Yang Y, et al. Cancer-targeted optical imaging with fluorescent zinc oxide nanowires. *Nano Lett*. 2011;11(9):3744–3750.
18. Anand B, Krishnan SR, Podila R, Sai SS, Rao AM, Philip R. The role of defects in the nonlinear optical absorption behavior of carbon and ZnO nanostructures. *Phys Chem Chem Phys*. 2014;16(18):8168–8177.
19. Podila R, Anand B, West JP, et al. Evidence for surface states in pristine and Co-doped ZnO nanostructures: magnetization and nonlinear optical studies. *Nanotechnology*. 2011;22(9):095703.
20. Egblewogbe M, Anand B, Podila R, Philip R, Siva Sankara Sai S, Rao AM. Defect induced changes in the linear and nanotetrapods. *Mater Express*. 2012;2(4):351–356.
21. Zhang HY, Ji ZX, Xia T, et al. Use of metal oxide nanoparticle band gap to develop a predictive paradigm for oxidative stress and acute pulmonary inflammation. *ACS Nano*. 2012;6(5):4349–4368.